Nonlocal sediment transport on steep lateral moraines, eastern Sierra Nevada, California, USA

Tyler H. Doane [1], David Jon Furbish[1,2], Joshua J. Roering[3], Rina Schumer[4], and Daniel J. Morgan[1]

[1]Department of Earth and Environmental Sciences, Vanderbilt University, Nashville, Tennessee, USA
[2]Department of Civil and Environmental Engineering, Vanderbilt University, Nashville, Tennessee, USA
[3]Department of Earth Sciences, University of Oregon, Eugene, Oregon, USA
[4]Division of Hydrologic Sciences, Desert Research Institute, Reno, Nevada, USA

Key Points:

- Numerical models involving nonlocal transport closely match observed moraine profiles.
- The parameters of nonlocal models have clear physical definitions and entrainment is a key value.
- The evolution of the land-surface spectra based on different transport formulae are diagnostic of the style of sediment transport.

Corresponding author: Tyler H. Doane, tyler.h.doane@vanderbilt.edu

Abstract
Recent work has highlighted the significance of long-distance particle motions in hillslope sediment transport. Such motions imply that the flux at a given hillslope position is appropriately described as a weighted function of surrounding conditions that influence motions reaching the given position. Although the idea of nonlocal sediment transport is well grounded in theory, limited field evidence has been provided. We test local and nonlocal formulations of the flux and compare their ability to reproduce land-surface profiles of steep moraines in California. We show that nonlocal and nonlinear models better reproduce evolved land-surface profiles, notably the amount of lowering and concavity near the moraine crest and the lengthening and straightening of the depositional apron. The analysis provides the first estimates of key parameters that set sediment entrainment rates and travel distances in nonlocal formulations, and highlights the importance of correctly specifying the entrainment rate when modeling land-surface evolution. Moraine evolution associated with nonlocal and nonlinear transport formulations, when described in terms of the evolution of the Fourier transform of the moraine surface, displays a distinct behavior involving growth of certain wavenumbers, in contrast to the decay of all wavenumbers associated with linear transport. Nonlinear and nonlocal formulations share key mathematical elements yielding a nonlinear relation between the flux and the land-surface slope.

1 Introduction

Recent work on hillslope sediment transport has highlighted the idea that sediment particle travel distance is an important component of the flux [*Michaelides et al.*, 2010; *Lamb et al.*, 2011; *Shelef and Hilley*, 2016; *Carretier et al.*, 2016]. In certain settings, transport processes may redistribute sediment over length scales that are long relative to hillslope topographic (e.g., slope) length scales. These situations require nonlocal formulations for the hillslope sediment flux. That is, the flux at a position x [L] is a weighted function of the conditions around x. This class of nonlocal models differs significantly from more common local models that assume particle motions are much smaller than the length scales over which hillslope properties change. Local models suggest that the flux may be described as a function of local conditions at x whereas nonlocal models stipulate that distal conditions contribute to the flux at x. Previous research has focused on the theoretical development of nonlocal descriptions of flux that explicitly include the effect of long-distance particle motions [*Foufoula-Georgiou et al.*, 2010; *Tucker and Bradley*, 2010; *Furbish and Haff*, 2010; *Furbish and Roering*, 2013] and has highlighted the mathematical difference between local and nonlocal models. Existing literature presents compelling reasons to use nonlocal formulations for the hillslope sediment transport. It shows that nonlocal fomulations reproduce steady-state topographic profiles [*Foufoula-Georgiou et al.*, 2010; *Furbish and Haff*, 2010], are theoretically sound, and contain parameters that are physically based and potentially measurable [*Furbish and Roering*, 2013]. We augment existing work by demonstrating nonlocal transport and its consequences in a field setting at the hillslope scale. Demonstrating nonlocal transport requires that we first distinguish between nonlocal and local formulations.

The mathematical distinction between nonlocal and local sediment transport is well-defined. However, a physical distinction may be obscured by the presence of a suite of processes that transport sediment over various length scales [*Furbish and Roering*, 2013]. For example, the lengths of disturbance-driven particle motions due to shrink-swell, freeze-thaw cycles and localized bioturbation are on the order of the pore diameters (or perhaps many pore diameters) within the soil column. The lengths of particle motions on the soil surface produced by rain splash are on the order of millimeters to decimeters. These quasi-random motions in the soil column or on its surface result in a bulk downslope motion whose rate is approximately proportional to the local land-surface slope [*Culling*, 1963; *Carson and Kirkby*, 1972; *Fernandes and Dietrich*, 1997; *Jyotsna and Haff*, 1997; *Furbish et al.*, 2009a]. In contrast, processes such as dry ravel, shallow landslides, tree throw, patchy surface flows and the activity of fossorial animals may involve transport distances that are on the order of

meters if not much longer. This is particularly true in steepland settings where particle transport distances increase [*Gabet et al.*, 2003; *Gabet and Mendoza*, 2012]. On any given hillslope, a suite of individual transport mechanisms with different characteristic length scales may compose the aggregate sediment transport. Length scales of particle motions for these processes may blend smoothly or discretely from short (pore scale) to long (many meters), complicating a physical distinction between local and nonlocal transport. Thus, identifying behaviors and characteristics of transport formulations, and their veracity when applied to field conditions, is clouded by the variability of length scales of natural transport processes. In this paper, we overcome this difficulty by evaluating the long-term evolution of geomorphic features.

Directly observing natural sediment transport on hillslopes usually requires being in the right place at the right time, and, except for field-based plot-scale experiments or at instrument-deployed sites, direct measurements of transport are unusual if not impossible over large areas and timescales. At climate-change and longer timescales, we have no choice but to consider how the time-integrated effects of transport are reflected in land-surface geometry, possibly including additional soil constituents whose behaviors are coupled with surface evolution [*Furbish*, 2003; *Roering et al.*, 2004; *Johnson et al.*, 2014; *Anderson*, 2015]. In certain situations, the hillslope form and land-surface evolution may reflect the time-averaged characteristics of transport. We believe this to be the case for our descriptions below of transport and the post-depositional evolution of lateral moraines that emerge from the eastern front of the Sierra Nevada, California, USA. These moraines provide an ideal opportunity to evaluate different transport formulae because they have well-defined ages and initial conditions.

Specifically, we use local linear [*Fernandes and Dietrich*, 1997; *Mudd and Furbish*, 2007], local nonlinear [*Roering et al.*, 1999; *Ouimet et al.*, 2009; *DiBiase et al.*, 2010] and nonlocal [*Furbish and Haff*, 2010; *Furbish and Roering*, 2013] formulations of hillslope sediment transport to numerically simulate the evolution of these steep lateral moraines. The analysis reveals two significant items. First, based on numerical analyses we show that nonlocal models mimic moraine profile evolution with higher fidelity than local, linear diffusion. To our knowledge, this is the first demonstration that documents nonlocal hillslope sediment transport at the hillslope scale using the class of models described below. Nonlocal models match the performance of nonlinear models and we argue that these models share low-order mathematical form, and are therefore expected to perform similarly. We are able to make the first estimates of the numeric values of parameters that are central to the nonlocal formulation and reflect real physical and measurable components of sediment transport. The parametric values we extract are likely specific to the lateral moraines because glacial till contains such a wide range of grain sizes and moraines are entirely composed of unconsolidated sediment. However, so long as the landscape is transport-limited, similar values may apply to the region due to regional climate and ecology. Second, we are able to identify a distinct mathematical behavior of nonlocal and local nonlinear formulations for sediment transport. In particular, we observe that the evolution of the Fourier transform of the land-surface elevation shows amplification in certain wavenumbers k ($k = 2\pi/L$ where L is the wavelength) for nonlocal and nonlinear models. This differs from the behavior associated with the linear "diffusive" description of the flux normally adopted for convenience in landform/landscape evolution models, which necessarily results in spectral decay of all wavenumbers. In addition we show that simplified versions of nonlocal and nonlinear flux models share mathematical similarities leading to similar behavior under certain conditions.

In section 2 we review the concepts of local linear, local nonlinear and nonlocal sediment transport and we present modifications to formulations suggested by previous authors. Section 3 describes the setting, glacial history and characteristics of the lateral moraines used in the study. In section 4 we focus on numerical methods. Results showing that nonlocal transport effectively accounts for the evolution of the land surface are presented in section 5. Here we also present a basic description of the time-evolution of the Fourier transform of the

land-surface elevation. A full treatment of this spectral behavior is beyond the scope of this paper, but the results indicate value in using the evolution of Fourier transforms to clarify key elements of land-surface evolution.

2 Theory

2.1 Local Linear Transport

For disturbance-driven transport involving relatively short particle motions — whether due to the continual creation and collapse of porosity within the active soil thickness or to surface transport by rain splash — the volumetric flux $q(x)$ [$L^2\ T^{-1}$] often is described by a linear, slope-dependent transport model, namely [*Culling*, 1963; *Fernandes and Dietrich*, 1997; *Jyotsna and Haff*, 1997; *Carson and Kirkby*, 1972; *Tucker and Bras*, 1998],

$$q(x) = -D\frac{\mathrm{d}\zeta}{\mathrm{d}x} = -DS, \tag{1}$$

where ζ [L] is the land-surface elevation, D [$L^2\ T^{-1}$] is a diffusivity-like rate constant, and the land-surface slope $S = \mathrm{d}\zeta/\mathrm{d}x$. This is by definition a local formulation of transport. The surface slope S is defined locally at a scale larger than the disturbance-driven motions, and it is assumed that these motions (locally) are uninfluenced by variations in soil or land-surface conditions over distances longer than the scale used to define the slope. The linear slope dependency represents the lowest order effect of gravity in producing a downslope bias in motions of soil particles. Process oriented formulations have confirmed the slope dependency [*Furbish et al.*, 2009a,b; *Anderson, R.S.* , 2002; *Dunne et al.*, 2010]

2.2 Local Nonlinear Transport

There is evidence that the volumetric sediment flux is nonlinearly related to the land-surface slope [*Ouimet et al.*, 2009; *DiBiase et al.*, 2010]. For example, *Roering et al.* [1999] developed a nonlinear model with the form,

$$q(x) = -D\frac{S}{1-(|S|/S_c)^2}, \tag{2}$$

where S_c is a critical slope. As the magnitude of the land-surface slope approaches S_c, the flux q mathematically approaches infinity. The behavior of (2) at slopes below S_c is consistent with data of hillslope form [*Roering et al.*, 1999, 2007] and erosion rates. To create a nonlinearly slope-dependent flux, this model partially calls on increasing sediment transport distances involved with small landslides and ravel. However, given that (2) is a local function of x, the model does not explicitly include long-distance sediment motions.

Nonetheless, in relation to our comparison below of the nonlinear model (2) with nonlocal formulations of transport, we note that both are motivated by the same idea: on steep slopes, long-distance motions become a significant component of the flux. As described in the next section, the difference between these models is the treatment of particle motions. In addition, whereas nonlocal models may in principle be adapted to short timescale problems, for example, sediment and nutrient delivery to channels, local nonlinear models effectively account for observed sediment fluxes and topographic configurations when averaged over much longer timescales, and necessarily require spatial averaging of the land-surface slope over scales of 7-10 meters [*Roering et al.*, 2010]. We suggest in Section 6.3 that nonlocal and nonlinear models share key mathematical attributes, namely, that they combine terms that are nonlinear in slope and therefore behave similarly for long timescale applications.

2.3 Nonlocal Transport

Several formulations have been proposed to describe nonlocal sediment transport on hillslopes. First, nonlocality can be introduced with a fractional calculus model where a

non-integer derivative of a quantity yields a nonlocal dependence [*Foufoula-Georgiou et al.*, 2010]. Second, rule-based models that follow particles or parcels of sediment downslope and evaluate a probability of continuing motion based on the local slope conditions result in long-distance motions [*Tucker and Bradley*, 2010]. A third model appeals to the sediment entrainment rate and the probability density function (pdf) of travel distance in order to describe the flux [*Furbish and Haff*, 2010; *Furbish and Roering*, 2013]. The pdf of travel distance describes the probability that particles move to within a distance r to $r + dr$ from the starting position. In this case the flux at x is a convolution integral-like [*Gilad and Von Hardenberg*, 2006] expression of sediment entrained at all surrounding positions x' weighted by the probability that it travels at least a distance $x - x' = r$, thereby contributing to the flux at x. Mathematically this is expressed as,

$$q(x) = \int_{-\infty}^{x} E(x')R(x - x'; x')\,\mathrm{d}x', \tag{3}$$

where $E(x')$ [$\mathrm{L}^3\ \mathrm{L}^{-2}\ \mathrm{T}^{-1}$] is a volumetric entrainment rate, R is a kernel related to the probability density function of $f(r, x')$ of travel distances $r = x - x'$, and x' is an upslope position. On a hillslope where slopes vary as a function x', $R(x - x', x')$ should reflect the increasing probability of long distance motions on steeper slopes [*Gabet and Mendoza*, 2012]. The flux then is a unique result of the particular configuration of slopes around x. We use (3) as the general formulation for the flux throughout this paper, because the volumetric entrainment rate and a probability density function of particle travel distance are two physically interpretable and potentially measurable components. This approach also complements research that focuses on estimating the particle travel distance of various transport processes [*Gabet*, 2003; *Furbish et al.*, 2009b; *Michaelides et al.*, 2010; *Gabet and Mendoza*, 2012; *DiBiase et al.*, 2017].

Nonlocal hillslope sediment transport models have been primarily developed for transport-limited conditions. However, a particularly appealing characteristic of a flux formulation like (3) is that it may be applied to detachment limited conditions as well. In this case, the entrainment rate, E, becomes the rate of detachment as opposed to the entrainment of unconsolidated regolith. In this situation, the functional form of $E(x')$ may be different from what is presented below. Nonetheless the mathematical framework would be the same. Furthermore, similar transport theories may apply to fluvial sediment transport [*Parker et al.*, 2000; *Furbish et al.*, 2012; *Martin et al.*, 2012; *Fathel et al.*, 2015; *Heyman et al.*, 2016]. Therefore, this type of description of the flux opens opportunities to examine commonalities between transport on hillslopes and in rivers.

2.3.1 Entrainment Rate

The entrainment rate E [$\mathrm{L}^3\ \mathrm{L}^{-2}\ \mathrm{T}^{-1}$] represents a volume of sediment set in motion per unit area during a time interval $\mathrm{d}t$. There are likely different and valid functional forms for $E(x')$ that reflect natural entrainment processes. For example, entrainment by rainsplash is uniform when averaged over long times relative to a shifting ground cover. In contrast, the incidence of tree throw may increase with increasing slope [*Hellmer et al.*, 2015], which implies a slope dependency in the entrainment rate. A general functional description of the entrainment rate is

$$E(x') = E_0 + E_1|S|^{\alpha}, \tag{4}$$

where E_0 [$\mathrm{L}^3\ \mathrm{L}^{-2}\ \mathrm{T}^{-1}$] is a uniform background entrainment rate and E_1 [$\mathrm{L}^3\ \mathrm{L}^{-2}\ \mathrm{T}^{-1}$ is a slope-modulated term. For simplicity, Furbish and Haff [2010] set $\alpha = 1$. Here, we explore the possibility that $\alpha \neq 1$.

For the analyses presented below, we set $E_0 = 0.001$ m yr^{-1} as a constant in order to limit the fitting of parameters, and then appeal to previous work suggesting that E_1 is larger [*Furbish and Haff*, 2010]. Setting $E_0 = 0.001$ m yr^{-1} is based on the amount of degradation at the ridge top. Over the 40 ka of evolution, this value of E_0 suggests that 40 m of material has been entrained. However, the bulk of that material remains at the ridge. We expect that

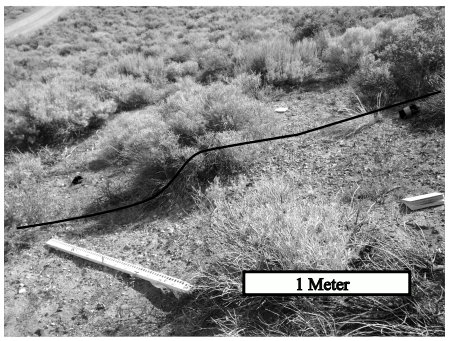

Figure 1. Image of shrub showing its behavior as a sediment capacitor with upslope sediment storage and over-steepened downslope side. The black line represents a trace of the land-surface.

E_0 may vary from 0.001 m yr^{-1}, however, we think that we are within an order of magnitude of the actual value because lowering due to the divergence of the flux at the ridge is necessarily less than 40 m. If E_0 is too low, then the value of E_1 can largely make up the difference on sloped terrain. If the value of E_0 is too large, then E_1 can not counteract the excess flux. Therefore, we think a value of 0.001 m yr^{-1} is a conservative estimate. Furthermore, insofar as this paper is aimed at demonstrating nonlocal transport from land-surface form and E_0 is a constant regardless of profile form, fitting this quantity as a free parameter adds little or no insight to the behavior of the moraine surface. That is, the value of E_0 has little impact on the form of the evolving moraine, although it does influence the magnitude of the flux, and therefore will influence the magnitude of other parameters that we fit. We must interpret the parametric values as being influenced by our choice of values for E_0.

The motivation for a nonlinear functional form for $E(x')$ comes from the observation that obstacles on hillslopes both trap and route sediment downslope [*Furbish et al.*, 2009b; *DiBiase and Lamb.*, 2013; *Lamb et al.*, 2013] (Figure 1). These are essentially no-flux obstacles where sediment accumulates on the upslope side and is eroded from the downslope side. This has the important effect of over-steepening the land-surface immediately downslope of the obstacle. We suggest that when the obstacles are removed, the trapped sediment is available for transport and ravels downslope [*DiBiase and Lamb.*, 2013]. The volume of sediment that is released depends on the volume of sediment that is trapped in a wedge upslope of the over-steepened portion (Figure 2). Immediately below an obstacle we typically observe a minor depression that would act to locally disentrain sediment. However, the depressions are often small in comparison to the mounds that form upslope. Furthermore, disentrainment does not bear on the volume of entrained sediment. This is only one mechanism for producing a nonlinear relationship between entrained sediment volume and land-surface slope and we expect that there are likely many processes (i.e. [*Michaelides et al.*, 2012]) that share this type of relationship.

To obtain a functional form of E for this process we approximate the volume of the over-steepened wedge in relation to the land-surface slope. To do so, we approximate the flux near a downslope no-flux obstacle with linear diffusion, which produces an over-steepened surface. Linear diffusion is used here purely for illustration purposes to generate mounds that resemble those observed in the field. We do not suggest that sediment transport is entirely described by (1). We then define a three-dimensional wedge with a bottom surface that extends from the base of the over-steepened step up-slope to the land-surface and is inclined at the angle of repose (Figure 2A). Results from this simulation show a nonlinear relationship between the entrained volume and the land-surface slope (Figure 2B) [*Putkonen et al.*,

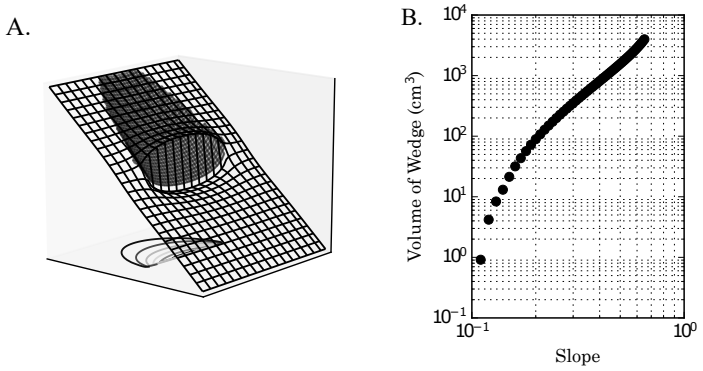

Figure 2. Schematic diagram showing how the volume of entrained material increases nonlinearly with slope. Contour lines (A) show the thickness of the wedge of sediment available for ravel, with calculations of the volume entrained as a function of slope (B).

2012]. The volume-slope relationship represents an idealized case whereas in reality mound geometry varies, and we expect some deviation from the relationship presented in Figure 2B. Nonetheless we suggest that this analysis captures the nonlinearity of the relationship, which is central in determining the functional form of $E(x)$. For slopes between 0.1 and 0.7, the entrained volume appears to be well-approximated by a power relationship somewhere between S^2 and S^3. For simplicity, we use a squared relationship,

$$E(x') = E_0 + E_1|S(x')|^2, \tag{5}$$

where E_1 represents effects of obstacle density and removal rate. E_0 represents the rate of entrainment due to slope independent processes such as rain-splash or lofting due to freeze-thaw. Here we assume that obstacles are uniformly distributed and their mean duration is constant. Therefore, obstacle removal rate in E_1 sets the time-scale and gives it the dimensions [L T^{-1}].

Building sediment capacitors requires a sufficient amount of time for the obstacle to accumulate sediment. The early evolution of the moraine in this case, then, had some spin-up time during which the initial capacitors were constructed. The timescale for capacitor construction is much shorter than that for the moraine evolution and is insignificant in terms of land-surface morphology. The spin-up time may become significant for small landforms where capacitors are relatively large.

The capacitors at our field site are Sage brush. We note that the argument above is specific to the idea of storage and release of sediment by shrubs, while acknowledging the possibility of a changing ecology and climate during the period of moraine evolution [*Mensing*, 2001]. Nonetheless, we speculate that this period, except immediately following glacier recession, likely involved the continuing occurrence of vegetation with similar effects on transport. Furthermore, we suggest that vegetative sediment capacitors is one mechanism for a nonlinear formulation of E with slope, although there may be other processes with nonlinearly slope-dependent entrainment rates. With this uncertainty, we must view the fitting of moraine profiles in relation to the nonlocal formulation of transport as an hypothesis, and we note that the model testing described below includes a linearly and nonlinearly slope-dependent form for E.

2.3.2 Travel Distance

The kernel-like term in (3), $R(x - x', x')$, is the survival function of the pdf $f(r, x')$, where $R = 1 - \int_0^r f(r, x')\,\mathrm{d}r$. Previous research [*Furbish and Haff*, 2010; *Furbish and Roering*, 2013] has used an exponential pdf for several reasons. First, comprehensive empirical data that reflects travel distances of the suite of processes that might occur on hillslopes is limited. However, we heuristically imagine that most particles move short distances while a few will travel far — a general behavior captured by exponential functions. We note that power-law functions share this behavior and we address this below. Second, exponential distributions have simple expressions for their statistical moments, which has proven useful in approximating nonlocal behavior in advection-diffusion form [*Furbish and Haff*, 2010]. In contrast, power-law distributions often have undefined statistical moments. Third, an exponential distribution reflects the notion that arresting a particle in motion is a Poisson process where over any interval of space, particles in motion have constant probability of stopping. Rock-drop experiments show that travel distances are distributed exponentially and that a friction model performs well in simplified conditions [*Kirkby and Statham*, 1975; *Gabet and Mendoza*, 2012; *DiBiase et al.*, 2017]. This idea leads to the conceptualization of a decay constant (e.g., the mean of an exponential distribution) which we recast as a spatial disentrainment rate that describes the proportion of sediment that stops over a given distance. This allows us to begin with a physically based although simple conceptualization of the bulk motion of sediment.

Previous authors have suggested that kernels with exponential forms result in landscape evolution that is consistent with local linear diffusion [*Foufoula-Georgiou et al.*, 2010]. Whereas this analysis is correct for uniform kernels, the flexibility offered in (3) can result in unique nonlocal behaviors while using exponential distributions of travel distance. Including the function $E(x')$ in (3) also leads to unique behavior. That is, the volumetric entrainment rate and the mean particle travel distance can vary as a function of land-surface conditions, which leads to unique behaviors using an exponential pdf for travel distance. The flux in this case becomes a linear combination (exponential weighting by $R(x - x', x')$) of surrounding values for the volumetric entrainment rate ($E(x')$). We also suggest that although under certain conditions exponential kernels lead to behaviors described by local transport, (3) explicitly relates sediment contributions from different locations on a hillslope and is inherently nonlocal.

The concept of disentrainment is treated in previous research [*Furbish and Roering*, 2013]; however, we briefly outline the physical interpretation here. Generally, disentrainment describes the probability that a particle or portion of sediment set in motion at x' at time t moves to an interval $r = x - x'$ to $r + \mathrm{d}r = x - x' + \mathrm{d}x$ at time $t + \mathrm{d}t$. This rate does not define the particular path taken by each particle or proportion of the entrained volume. Rather, particles may take any number of motions to get to $x = x' + r$ at $t + \mathrm{d}t$. This concept reflects the notion that there may be a suite of processes transporting particles downslope and that a single particle may experience motion due to any number of processes several times during the interval $\mathrm{d}t$. This simplifies the problem into a purely probabilistic one in which the pdf of travel distance simply represents the distribution of particle positions after a given time $\mathrm{d}t$. By allowing for the possibility of particle travel distance to be a result of multiple hops we are in effect considering a discrete process. However the mathematics that we use are continuous in time and space. For this reason the entrainment rate and pdf of particle travel distance must be time-averaged quantities [*Furbish and Haff*, 2010; *Furbish et al.*, 2012], such that the pdf of travel distances represents a distribution of transition probabilities associated with the interval $\mathrm{d}t$.

The development of a disentrainment rate is based on two ideas common in hillslope sediment transport. First, empirical data suggest that particle transport distances increase on steeper slopes for a host of processes [*Gabet et al.*, 2003; *Furbish et al.*, 2009b; *Dunne et al.*, 2010; *Gabet and Mendoza*, 2012]. Second, hillslope sediment flux nonlinearly increases as land-surface slopes approach a critical slope, S_l [*Roering et al.*, 1999; *Ouimet et al.*, 2009;

DiBiase et al., 2010]. This implies that the sediment particle travel distance nonlinearly increases with slope, or the spatial disentrainment rate nonlinearly approaches zero. Combining these constraints we can describe a disentrainment rate, $P(x')$ [L^{-1}], that is slope-dependent and goes to zero when $|S| \rightarrow S_l$,

$$P(x') = \frac{1}{\lambda_0}\left[\frac{2S_l}{S_l - S(x')} - 1\right] \quad -S_l < S < 0, \tag{6}$$

where λ_0 is a characteristic length scale and $S(x')$ is the local land-surface slope which carries sign. In this case, S_l represents the slope at which particle motions continue indefinitely, and differs from the definition of the critical slope S_c which is the slope at which the flux becomes unbounded. When $S \rightarrow S_l$, the flux is simply the entirety of what is entrained, and therefore the flux does not approach infinity. So long as $S << S_l$, the actual value of S_l has little impact on the flux values calculated. The mean travel distance is $1/P(x')$, which has a nonlinear relationship with slope and is consistent with experimental results of particle travel distances [*Gabet and Mendoza*, 2012]. For an exponential pdf of travel distances,

$$f(x - x', x') = \frac{1}{\lambda_0}\left[\frac{2S_l}{S_l - S(x')} - 1\right] e^{-\frac{x-x'}{\lambda_0}\left[\frac{2S_l}{S_l - S(x')} - 1\right]}. \tag{7}$$

Using the relationship between f and R we get

$$R(x - x', x') = 1 - \int_0^x f(x - x', x')\mathrm{d}x' = e^{-\frac{x-x'}{\lambda_0}\left[\frac{2S_l}{S_l - S(x')}\right]}, \tag{8}$$

which describes the probability of sediment traveling at least a distance $x - x'$ such that it contributes to the flux at x. Inserting (8) for $E(x')$ into (3), we obtain the flux in the positive x direction

$$q_p(x) = \int_{-\infty}^{x} \left[E_0 + E_1|S(x')|^{\alpha}\right] e^{-\frac{x-x'}{\lambda_0}\left[\frac{2S_l}{S_l - S(x')}\right]} \mathrm{d}x', \tag{9}$$

This expression represents the downslope component of the flux; however, there is a possibility that the net flux will involve an upslope component.

2.3.3 Bi-directional motions

Processes such as rainsplash [*Furbish et al.*, 2009b; *Dunne et al.*, 2010] and transport due to fossorial animals [*Gabet et al.*, 2000, 2003] distribute sediment both downslope and upslope. The proportion, p, of downslope transport and the proportion, n, of upslope transport may be specified by

$$\begin{aligned} p(x') &= \tfrac{1}{2}\left[1 - \tfrac{S(x')}{S_p}\right] && -S_p \le S \le S_p \\ p(x') &= 1 && -S > S_p \\ p(x') &= 0 && -S < -S_p \\ n(x') &= 1 - p(x'), \end{aligned} \tag{10}$$

where S_p is a threshold slope magnitude above which all sediment moves in the same direction. The flux in the negative direction involves convolving the negative-bound portion of entrained sediment with the survival function,

$$q_n(x) = \int_{\infty}^{x} n(x')E(x')e^{-\frac{x'-x}{\lambda_0}\left[\frac{2S_l}{S_l + S(x')} - 1\right]} \mathrm{d}x'. \tag{11}$$

The total flux is the sum of positive and negative contributions

$$q(x) = \int_{-\infty}^{x} p(x')E(x')e^{-\frac{x-x'}{\lambda_0}\left[\frac{2S_l}{S_l - S(x')} - 1\right]} \mathrm{d}x' + \int_{x}^{\infty} n(x')E(x')e^{\frac{x'-x}{\lambda_0}\left[\frac{2S_l}{S_l + S(x')} - 1\right]} \mathrm{d}x'. \tag{12}$$

The net flux according to (12) on a flat surface is zero as positive and negative motions cancel each other. As slopes steepen, downslope motions make up a larger component of the entrained volume and travel distances increase (Figure 3).

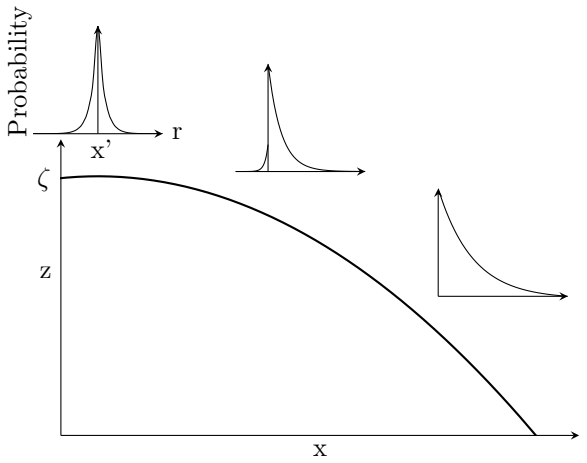

Figure 3. Schematic diagram of a hillslope profile $\zeta(x)$ showing the partitioning of positive and negative motions starting from a position x' and how the probability density function of particle travel distances r changes as a function of local slope.

Although the downslope component of the flux is expected to dominate at our field site, the presence of an upslope component changes the slope-dependency. That is, the slope dependency of n and p, which contain $S(x')$, adds another slope-dependent term. Therefore, the impact of the upslope flux, although small, may be observed in hillslope form. We expect this to be particularly true on low-angle slopes, or at ridge-tops where the magnitude of concavity is large.

3 Moraine Evolution

Moraines can be useful landforms for testing sediment transport formulations because they have a well-constrained initial condition [*Putkonen et al.*, 2008] and their depositional ages are estimated from exposure-age dating techniques. This allows us to use a specified model, starting from the initial condition, to simulate the evolution of the moraine over its age. The outputs of these numerical models can be compared with the observed condition to evaluate the performance of sediment transport formulations.

We focus on the evolution of the interior of lateral moraines because they are better preserved than terminal moraines which are often degraded by fluvial processes. Although there is some uncertainty with regard to the depositional age of moraines, typical age ranges of thousands of years [*Rood et al.*, 2011] do not significantly affect the results and implications presented below. The general evolution of a lateral moraine is as follows. While the associated glacier is active, the lateral moraine is buttressed by the ice that it contains, which allows for the interior side to oversteepen. Following the retreat of the glacier, the moraine quickly relaxes to the angle of repose, which for glacial till is ~ 0.67 [*Putkonen et al.*, 2008]. We assign the exposure-age of the moraine to this condition and numerically simulate the subsequent evolution of the moraine by the proposed sediment transport formula.

The moraines on the east side of the Sierra Nevada, California, are particularly well-suited for this type of study for several reasons. First, they often emerge from the mountain front and are deposited in the adjacent basins. This configuration allows for moraines to be completely unconfined and the form is not conditioned by the geometry of valley walls or floors. Therefore, the form of the moraine is only a result of the initial condition, its age, and sediment transport. Second, the glacial chronology of this region is well studied [*Schaefer et al.*, 2006; *Phillips et al.*, 2009; *Rood et al.*, 2011], which provides estimates for the ages

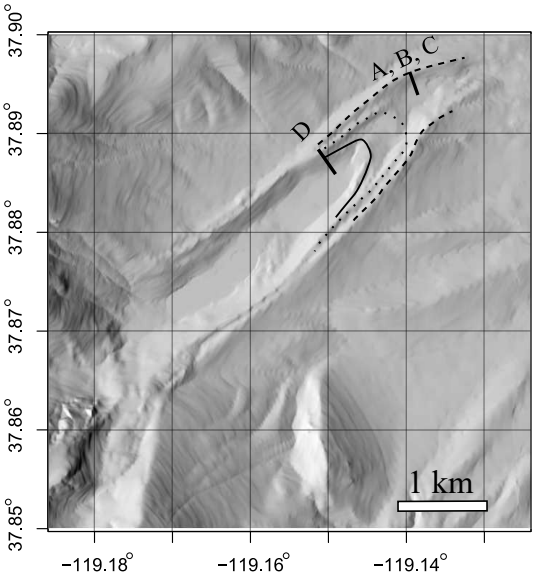

Figure 4. Hillshade image of Bloody Canyon, California with traces of Tahoe (40 ka, dashed line [*Schaefer et al.*, 2006; *Kaufman et al.*, 2003]), Tioga 1 (25 ka, dotted line [*Kaufman et al.*, 2003]), and Tioga 3 (18 ka, solid line [*Morgan and Putkonen*, 2012; *Rood et al.*, 2011]). Locations and orientations of profiles A, B, C and D are shown.

of deposition. Third, these moraines have large side-slope lengths of ~120 m, which we may assume is much larger than typical sediment particle displacements. A great number of particle displacements are responsible for the observed moraine form; thus large moraines represent a greater "sampling" of particle motions than smaller landforms.

The moraines on the eastern side of the Sierra Nevada record a suite of glacial advances and retreats. Last Glacial Maximum advances are represented by the Tioga (14-25 ka) [*Kaufman et al.*, 2003] moraines and penultimate glaciations are represented by the Mono Basin (92-119 ka [*Phillips et al.*, 1990] or 60-80 ka [*Kaufman et al.*, 2003]) moraines. Between these two major glaciations is the Tahoe glaciation (42-50 ka) [*Kaufman et al.*, 2003]. For the purpose of this paper we specify an age for the Tahoe glaciation as 40 ka. For simplicity, we present the results from the youngest age estimate. We recognize that many authors suggest older ages for the Tahoe glaciation. Modeling results using 40 ka and 50 ka for initial conditions do not change the fit of models nor do parameters change significantly. Here we look at the post-glacial evolution of Tioga 3 and Tahoe lateral moraines that emerge from Bloody Canyon. Both are well preserved (Figure 4). The late Pleistocene glaciers in Bloody Canyon sourced granites and metasedimentary rocks in the Sierra Nevada to the west. The glacial till composed of these materials, particularly the granite clasts, weather into residual sand and gravel (Figure 1). Such coarse materials have high infiltration rates and concentrated overland flow and ponding of water on the surface is likely rare. Furthermore, because the moraines are composed entirely of porous unconsolidated sediment, there is no perched water table. These characteristics suggest that any localized surface flows are stochastic in space and time, thereby reducing the opportunity for concentrated rilling or incision. As such, the surfaces have remained relatively planar, which justifies a one-dimensional application of the numerical simulations. Planar surfaces are observed on all moraines, including those dated as Mono Basin (92-119 ka), which suggests that the moraines remain well-drained as they evolve.

A simple but significant observation is that the concentration of boulders changes as a function of position. Boulder concentration is high near the crest and approaches zero in

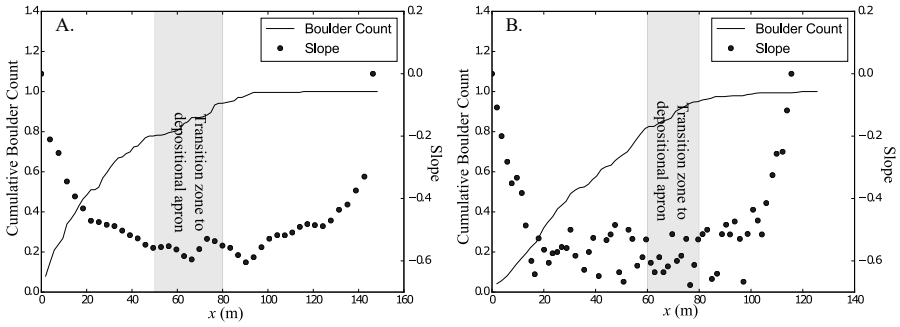

Figure 5. Plot of cumulative boulder count (lines) and surface slope slope (dots) as a function of horizontal position for profile C (A) and profile D (B). The depositional apron begins where the rate of boulder accumulation decreases.

the depositional apron of the moraine (Figure 5). In the apron we note that the surface is composed almost entirely of grusified gravels and sand that were presumably transported to the depositional apron. The boulders represent a coarse lag left behind as more mobile, finer-grained material moved downslope, such that with time the exposed boulder density increases at the crest and decreases near the toe [*Putkonen et al.*, 2008]. The presence of this lag and accompanying apron provides evidence that sediment transport occurs primarily over the surface of the moraine. Particles at the surface move when a disturbance occurs with sufficient energy to displace them. Disturbances with energy sufficient to move grains of sand and gravel occur far more frequently than those capable of moving boulders, and as such, finer material is moved downslope quickly, leaving behind a boulder lag. Although surface motions do not imply a certain transport formula, such motions are a requirement for nonlocal transport, as long-distance motions only occur on the surface. Consequently, we would expect to see a signature of nonlocal transport in this setting. We note that this may suggest an armoring effect during the evolution of the moraine, and we address this in the discussion in the context of nonlocal transport.

4 Methods

4.1 Field Methods

Using a self-leveling transit, we collected a high-resolution (2-3 m) topographic profile along the path of steepest descent down the interior flanks of the lateral moraines. At two to three meter intervals, we sampled at or above the typical spacing of sagebrush which dominates the ecology of the area. As described above, the shrubs act as sediment capacitors [*Furbish et al.*, 2009b; *Lamb et al.*, 2011, 2013] and locally add roughness elements to the land surface. Because our study is focused on the large-scale form of the moraine, we limited our sampling interval to the spacing of shrubs to avoid resolving roughness elements with greater detail. For each survey, we extended the profile from several meters down the exterior side of the crestline to several meters along the flat interior valley. In addition to collecting topographic data we also collected a count of boulders exposed on the surface as a function of downslope position. We conducted a high resolution count of boulders that were 25 cm or greater in diameter within 2×4 meter areas positioned along the profile. The boulder surveys were conducted along profile C (Tahoe) and D (Tioga 3). Profile C was collected for the purpose of a boulder survey so the resolution is coarser and the toe of the moraine is incompletely sampled. Nonetheless we include this profile in our analysis.

4.2 Numerical Methods

To evaluate local and nonlocal models of hillslope sediment transport, we have written three numerical procedures that simulate the evolution of moraines from their initial condition (slope at 0.67 [*Putkonen et al.*, 2012]) according to (1), (2), or (3). The models simulate the evolution of moraines over their specified ages and outputs are compared with observed moraine forms. Due to the mathematical distinction between local and nonlocal models, the numerical procedures differ significantly.

4.2.1 Surface evolution according to local linear transport

To evaluate the changing surface elevation, we substitute (1) into the Exner equation to obtain

$$\frac{\partial \zeta}{\partial t} = D\frac{\partial^2 \zeta}{\partial x^2}, \tag{13}$$

which is the familiar diffusion equation. Systems that evolve according to (13) are common in nature and the mathematical treatment of this problem is extensive [*Carslaw and Jaeger*, 1959; *Fernandes and Dietrich*, 1997; *Mudd and Furbish*, 2007; *Hornberger and Wiberg*, 2004]. The evolution of a moraine is a transient problem with a no-flux boundary at the crest and a long flat run-out in the interior valley floor. This problem may be simulated in two ways. The evolution may be modeled by iteratively calculating the change in elevation according to (13) through finite-differencing with proper treatment at the boundaries. Alternatively, we may analytically solve the evolution of the land-surface in the wave number domain through time using a Fourier transform. The evolution of the Fourier transform of a linearly diffusing land-surface has an analytical solution [*Carslaw and Jaeger*, 1959; *Schumer et al.*, 2009],

$$Z(k,t) = Z(k,0)e^{-k^2 Dt}, \tag{14}$$

where $Z(k)$ is the Fourier transform of the land-surface elevation, k is the wave number ($2\pi/L$ where L is wavelength), and t is time. Using this analytic expression allows us to compare modeled profiles and observed profiles directly with the specified moraine age without iterating through time steps. In order to satisfy the boundary conditions, we reflect the interior side of the moraine such that the slope at the crest remains zero.

We use (14) to find the value of D that produces the best fit between modeled and observed moraine forms. To quantify the fit, we define a cost function as the sum of squared differences between modeled and observed Fourier transforms of the moraine surface,

$$C_f(D) = \sum_{i=1}^{N} [Z_m(k) - Z_o(k)]^2, \tag{15}$$

where Z_m and Z_o are the Fourier transforms of the modeled and observed land surfaces respectively. We then use a Gauss-Newton iteration scheme to find the value of D that minimizes (15). Because (15) is a function of one variable and it is a quadratic, the solution that we iteratively determine is a global minimum and is necessarily the best-fit solution.

We note that over timescales of 10 ka or more, values of D are likely to vary as climate changes [*Hughes et al.*, 2009; *McGuire et al.*, 2014; *Madoff and Putkonen*, 2016]. At this time, however, we do not have information to justify choices of D through time. Furthermore, we demonstrate in Appendix A that, in the absence of external boundary forcing, the form of the land surface only reflects the time-averaged diffusivity. In this sense, the form of a moraine undergoing linear diffusion expresses no memory of changes in climate as might be reflected in changing diffusivity values.

4.2.2 Surface evolution according to local nonlinear transport

To numerically simulate the evolution of the moraine profiles according to a nonlinear flux formulation requires an iterative, finite-difference approach. To do so, we use Equation 9

in Roering et al. (1999), which places (2) into continuity. To identify the best-fit parameter, D, for this model, we simulate the evolution of the moraine profile over the specified age. We compare the modeled profile to the observed to obtain a misfit, which is used by a Gauss-Newton iteration scheme to pick a new value for D that minimizes the misfit. We note that S_c is also a tunable parameter, however, to avoid fitting too many parameters, we test $S_c = 0.8$ and $S_c = 1.2$, which represent two extreme possibilities.

4.2.3 Surface evolution according to nonlocal transport

The mathematical form of (3) is more complex than a local expression and we are unaware of an analytical solution such as (14). Therefore, modeling the evolution of a feature as a consequence of a convolution-like flux description is an iterative procedure. Note that the kernel in (3) varies with position so that the integral form of the flux is not a true convolution. This characteristic precludes us from making use of the convolution theorem for Fourier transforms which would significantly reduce the computational complexity. To find the best-fit parameters for a nonlocal formulation we numerically simulate the complete evolution of the moraine many times until the solution approaches a minimum of a cost surface, $C(E_1, \lambda_0)$. To make this process reasonable in terms of computational time, we developed a rapid algorithm to calculate the flux. To numerically encode (3) can require integrating over the entire $2N$ domain if there are positive and negative components to the flux. This results in an algorithm whose complexity is $O[2N^2]$ and is an inherently slow computational process. For large domains, this makes the brute-force method for calculating the flux slow. However, we follow a procedure [*Gilad and Von Hardenberg*, 2006] that can turn (3) into a true convolution by approximating the kernel.

The basic premise of the method is that the kernel function $R(x - x', x')$ is approximated by the sum of a series of N_l functions of the same form as $R(x - x', x')$, each weighted uniquely. The weights change as a function of position, thereby placing the spatial dependency of $R(x - x', x')$ on the weighting functions $w(x')$. This allows us to write

$$q(x) \approx \sum_{l=1}^{N_l} \int_0^x \kappa(x - x'; \phi_l) w_l(x') E(x') \, \mathrm{d}x' , \tag{16}$$

where $w_l(\phi, x')$ is a function that weights the approximating kernel $\kappa(x - x'; \phi_l)$, ϕ is the actual value of the parameter in the kernel, and ϕ_l is the value of the parameter in the approximating kernels. We can then divide (16) up into $h_l(x') = w_l(x')E(x')$ and $g_l = \kappa(x - x'; \phi_l)$ so that

$$q(x) \approx \sum_{l=1}^{N_l} h_l * g_l . \tag{17}$$

The convolution theorem for Fourier transforms can be applied to (17), as this is now in the form of a proper convolution. Upon inspection, the approximation of the flux produces nearly identical results as when (3) is encoded directly. The computational complexity of this process is $O[N_l N \log(N)]$, which for large domains is much smaller than the direct method.

An efficient algorithm that determines the surface evolution makes an iterative cost function minimization procedure possible. To find the set of parameters that minimizes $C_N(E_1, \lambda_0) = \sum(\zeta_i - z_i)^2$, we use a Levenberg-Marquadt descent procedure which marches down the cost-function surface until it reaches a minimum (Figure 6). In this case, the cost function is a nonlinear function of two variables, E_1 and λ_0, which could create local minima that would incorrectly identify the best-fit set of parameters. However, from observation we see that, for a variety of initial values of parameters, the Levenberg-Marquadt algorithm consistently leads to a similar minimum, which suggests that it is a global minimum (Figure 6) and that the results represent the best-fit parameters. The Levenberg-Marquardt algorithm fit only values for E_1 and λ_0 and kept the choice of $E_0 = 0.001$ constant.

We also did not parameterize S_l, although it is a tunable parameter in P. For slopes significantly less than S_l, λ_0 is the dominant variable determining the mean particle travel

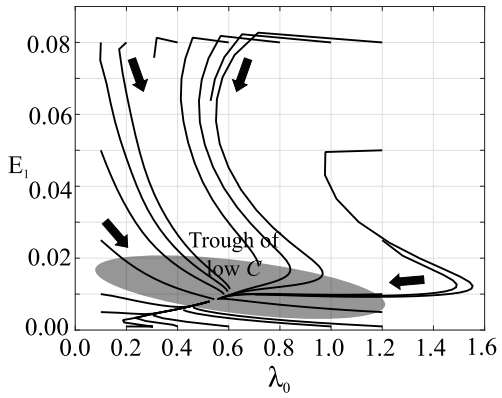

Figure 6. Two-dimensional plot showing the trajectory of parameters chosen by the Levenberg-Marquardt algorithm. All model runs started with initial parameteric values at the edge of the plot and iteratively march along the lines shown until the minimum is approached as denoted by the gray region. The common stopping place shared by all model runs suggests that the parameters presented here are the best-fit parameters and not a local minima.

distance, and therefore the flux. The presence of soil or regolith in transport-limited regimes suggests that the land-surface slope is well below the limiting slope, on which particles continue to travel indefinitely. Therefore, we may assume that S_l is significantly larger than slopes on the moraine surface such that errors associated with variations in the choice of S_l are relatively small.

We test three different nonlocal formulations against the surface evolution of lateral moraines. Case I is a nonlocal formulation with linearly slope-dependent entrainment and a downslope flux only. Case II has a linearly slope-dependent entrainment rate but with both upslope and downslope fluxes. Case III has a slope-squared dependency for entrainment and only downslope flux.

5 Results

5.1 Model Performance

We have tested six different transport models here, three of which are members of the nonlocal class but have either different functional forms for $E_1(x')$ or contain upslope and downslope contributions to the flux. Each of these models has two adjustable parameters, E_1 and λ_0, which are determined by the Levenberg-Marquadt procedure outlined above. In contrast, linear and nonlinear diffusion have only one free parameter, D (recall we test two separate values for S_c for nonlinear models).

Results from numerical experiments are summarized in Table 1. Nonlocal models more accurately predict profile forms than local linear diffusion as measured by the cost function. In general, nonlocal transport results in a cost, C_f, that is at least half of that generated by local linear models; however there is quite a bit of variation within the performance of nonlocal models themselves. Nonlocal models that contain positive and negative components of the hillslope sediment flux (Case II) are the worst-performing of the three tested here. A nonlocal flux model with linearly slope-dependent entrainment rate but only a downslope flux performs slightly better with a cost C that is about 40-60 points lower (Case I). Finally, a nonlocal formulation with nonlinear, slope-dependent entrainment rate and positive flux only (Case III) provides the best fit for all models. The cost C_f for this class of mod-

Table 1. Table of best-fit parameters and sum of squared differences for each profile as a result of nonlocal, local linear diffusion, and local nonlinear diffusion.

Profile	**A**	**B**	**C**	**D**	**Profile**	**A**	**B**	**C**	**D**
Age (ka)	~ 40	~ 40	~ 40	18	**Age (ka)**	~40	~40	~40	~18
Nonlocal Positive Flux Only					**Linear diffusion**				
$\sum(z-\zeta)^2$	129.00	64.99	127.33	83.22	$\sum(z-\zeta)^2$	385.80	320.44	329.00	184.5
E_1	0.005	0.0038	0.0042	0.0036	D	0.015	0.013	0.012	0.01
λ_0	0.65	0.75	0.57	0.61					
Nonlocal Positive and Negative Flux					**Nonlinear diffusion with $S_c = 1.2$**				
$\sum(z-\zeta)^2$	184.81	115.63	199.16	121.50	$\sum(z-\zeta)^2$	179.27	119.70	157.27	99.27
E_1	0.0037	0.0028	0.0025	0.0022	D	0.01	0.0096	0.0081	0.0076
λ_0	0.70	0.78	0.68	0.76					
Nonlocal Positive Flux with $E = E_0 + E_1 S^2$					**Nonlinear diffusion with $S_c = 0.8$**				
$\sum(z-\zeta)^2$	39.44	10.64	52.80	63.92	$\sum(z-\zeta)^2$	41.63	15.69	48.68	52.98
E_1	0.014	0.011	0.01	0.01	D	0.0061	0.0055	0.0046	0.0041
λ_0	0.32	0.37	0.30	0.40					

els is about an order of magnitude lower than local linear models on profiles *A*-*C*. In particular, consider profile *B* where case III results in $C \approx 10\ m^2$, more than an order of magnitude lower than linear diffusion (Figure 7). Note that C is a measure of the disagreement between the modeled topography, which is smooth and represents a time-averaged surface, and the observed topography which contains roughness elements and represents a moment in time. Because these roughness elements are not resolved in the numerical model, the cost C can never approach zero. Instead, the most successful model will approach some finite value of C that reflects the magnitude and spatial concentration of the roughness elements. Considering this, we suggest that these models are approaching the limit of C when the observed forms resolve the roughness elements and models do not. All models were run on a domain that represents 250 meters of horizontal distance. The side-slopes of the moraines are all different lengths; therefore, direct comparison between C_f for different profiles can not be done.

Local nonlinear models are capable of matching the abilities of nonlocal models to reproduce the observed profile form (Table 1). However, these nonlinear models require that the critical slope be around 0.8, which is significantly lower than values for the Oregon Coast Range [*Roering et al.*, 2007]. This value is not unreasonable, as S_c is thought to vary by a factor of 1.5. The sparse vegetation supported by the semi-arid climate of the Mono Basin lacks the vegetative anchors that are present in wetter areas which may contribute to lower critical slopes. Whereas these factors suggest that low S_c values may be expected, it is important to recognize that S_c is the slope at which the flux asymptotically becomes unbounded. Although critical slopes of 0.8 are possible, they are the lower limit of expected values. Furthermore, note that Figure 8A shows slopes that locally exceed 0.8, suggesting this location would have an unrealistically large flux in the absence of averaging over some spatial (or temporal) interval. This concept is addressed in the discussion.

The difference in model ability is highlighted by the residuals between modeled and observed profiles (Figure 9). At most locations on the moraine, the residual resulting from a nonlocal model is smaller than that of the linear model. In particular, nonlocal models per-

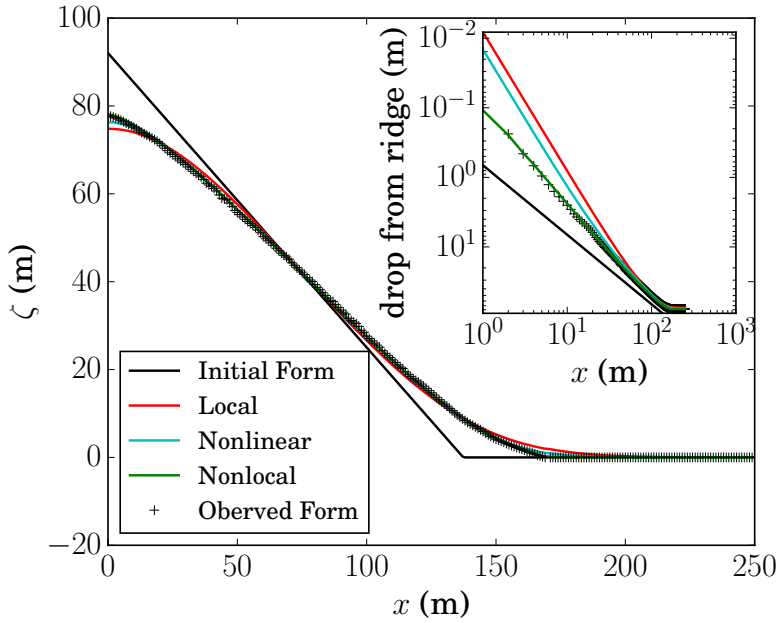

Figure 7. Plot of modeled (lines) and observed (crosses) land-surface elevation ζ versus horizontal position x. Drop-from-ridge plot (inset) highlights mismatch at the ridge of local models. The nonlinear model has $S_c = 0.8$ and the nonlocal model uses $E_0 + E_1|S|^2$.

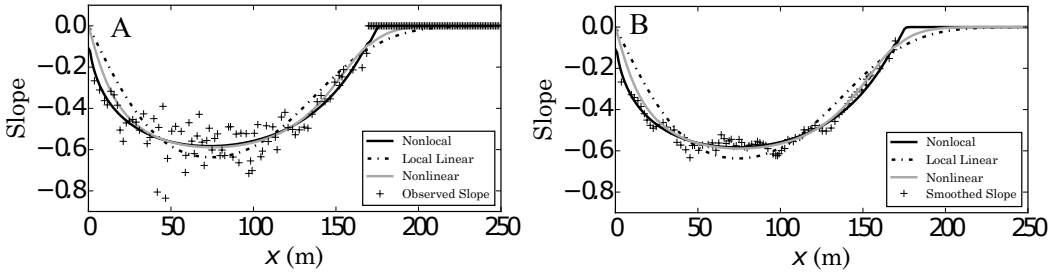

Figure 8. Plots of observed (crosses) and modeled (lines) land-surface slopes versus horizontal position for raw slope values (A) and smoothed values (B) using a 5-point moving average.

form better at the ridge and toes of the moraines. For example, in every model run, linear diffusion over-predicts erosion at the crest and extends the depositional toe further out. In some cases, linear diffusion over-predicts over 2.5 meters of erosion where nonlocal models fit quite well with residuals on the order of decimeters or less. The numerical fits are also highlighted in plots of land-surface slope from modeled and observed forms (Figure 8). These represent a more demanding fit than elevation residuals, and show that, relative to the local linear model, the nonlocal and local nonlinear models more closely fit the raw and smoothed values of slope, particularly near the crest (0 – 50 m), the mid-slope (70–80 m) and over the sediment apron (120 – 170 m).

The Levenberg-Marquardt algorithm that converges to a set of parameters that produce the best-fit topographic profile yields reasonable parametric values for nonlocal transport formulations. The most consistent estimates of parameters across profiles are generated by a slope-squared entrainment relationship (Case III). These values suggest that a slice of sediment from zero to one cm thick, depending on the slope, is entrained annually in this setting.

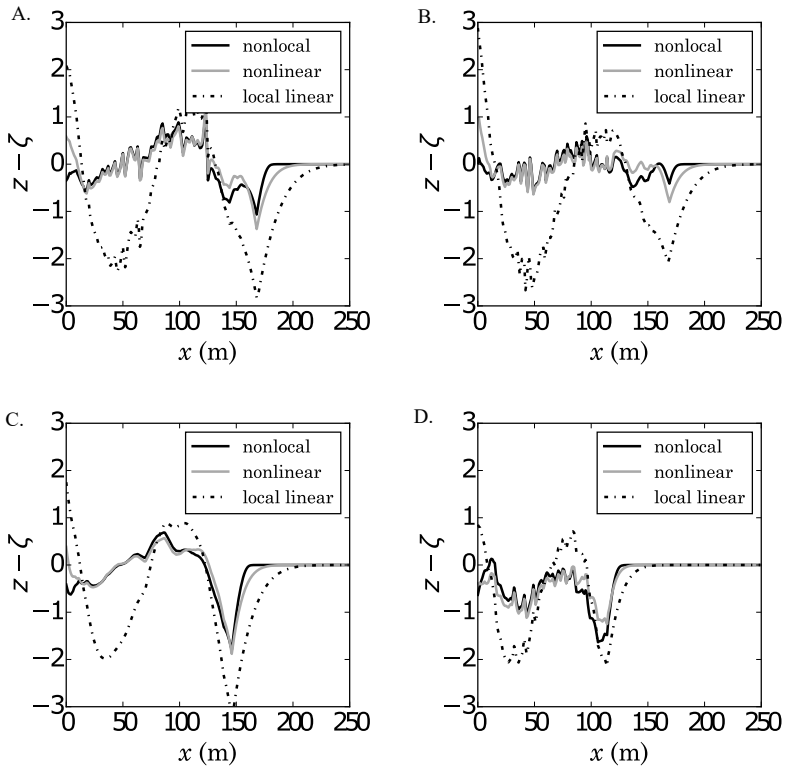

Figure 9. Plots of residuals between observed z and modeled ζ elevations versus horizontal distance x for moraine profiles A, B, C and D.

This is a time-averaged value, and at short timescales, we may observe isolated events that stochastically entrain far more (or less). Values for λ_0 are also consistent across profiles and suggest that mean travel distances $\mu_\lambda \approx 0.35/[2S_l/(S_l - S) - 1]$, or for $S \approx 0.6$, $\mu_\lambda \approx 1.2$ m.

5.2 Fourier Transforms

The application of Fourier transforms and their time evolution highlights distinct characteristics of nonlocal and linear processes. On inspection of (14) we note that there is only one possibility for the time evolution of the Fourier transform of a linearly diffusing medium. That is, the amplitude, $Z(k)$, of all wavenumbers can only decrease at a rate proportional to k and $Z(k)$. The amplitude at larger k decays faster than for smaller k, or in terms of wavelength, longer wavelength features persist for longer time. Whereas we see this behavior in the Fourier transform of the observed land surface for some wavenumbers, there are others that either grow or do not decay (Figure 10). Furthermore, linear diffusion predicts a much larger decrease in spectral amplitude in many wavenumbers, most notably, larger wavenumbers. Taken together, these observations simply and definitively illustrate that linear diffusion does not accurately account for the evolution of the moraine.

Whereas linear diffusion overestimates decay and is incapable of increasing spectral amplitude, nonlocal models can actually add spectral amplitude (Figure 10) in certain wavenumbers. That nonlocal models are capable of growing wavenumbers is consistent with the observed behavior. Furthermore, nonlocal models lead to growth in the same wavenumbers that have grown during the evolution of the moraine. Namely, the initial spectrum (gray) is shifted towards lower wavenumbers in both the observed and nonlocal spectra (black). To be clear, whereas we observe an increase in spectral amplitude in certain wavenumbers,

this is not to say that the system has added variance. Indeed, the variance of the land surface has decreased, but it is distributed differently among wavenumbers which results in select wavenumbers increasing in spectral amplitude. Spectra for profiles $B - D$ show a similar behavior, we have shown only one here for simplicity.

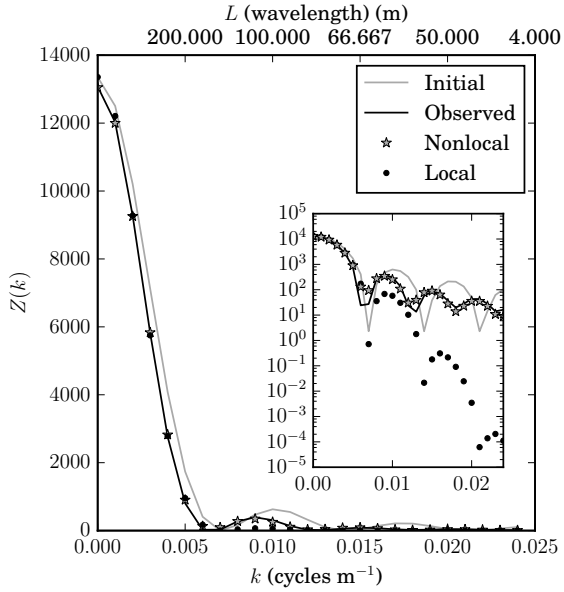

Figure 10. Fourier transforms of the observed (black line), modeled (circles and stars) and initial condition (gray line) of moraine profile A. Note that the wavenumber k has been divided by 2π. The inset is a semilog plot of the transform that highlights the transform at higher wavenumbers.

We emphasize that the finite spectral amplitudes over wavenumbers $0.007 < k < 0.02$ and $0.015 < k < 0.02$ in Figure 10 are part of the evolving basic structure of the moraine form. These local maxima represent the spectral amplitude that accounts for the large concavities at the ridge and toe of the moraine. The Fourier transform of a triangle contains local maxima and minima at wavenumbers that are related to the width of the triangle [*Poularikas*, 1998]. Therefore, local maxima not simply attributable to "noise" in the transform, and they are not at the high wavenumbers associated with localized roughness on the moraine surface (e.g., due to the roughness created by shrub mounds). As the spectrum of the land surface is shifted to lower wavenumber, it is like a triangle that is laterally stretched and vertically diminished. As such, the local maxima that remain in the spectrum represent an important, but relatively small portion of the variance that maintains a quasi-triangular form.

We pursue a full treatment of this spectral behavior separately; here we provide a summary of key elements relevant to our treatment of moraine evolution. The time-evolution of the growth rates of the Fourier spectrum is of particular interest as it may provide a tool to decipher the roles of nonlocal/nonlinear versus local, linear transport. Figure 11 shows how positive growth rates of the spectrum change as the simulated moraine evolves according to nonlocal transport. Early evolution is marked by fast growth rates in high wavenumbers (short wavelength) for short periods of time that give way to more persistent but slower growth in lower wavenumbers (longer wavelength). This is not surprising as low wavenumber (long wavelength) features simply represent more mass. This type of transfer of spectral amplitude is known of as an inverse spectral cascade [*Domaradzki and Rogallo*, 1990]. With

continued evolution, the positive growth rates asymptotically approach zero, and the temporal evolution of the Fourier spectrum then is close to what is expected for linear diffusion. Note that spectral growth rates co-evolve with the land-surface slope and concavity, and in particular as slopes and concavities are reduced, positive growth rates are reduced. Therefore, certain topographic configurations (e.g., those with steep slopes and sharp concavities), nonlocal and local, nonlinear formulations lead to fundamentally different Fourier evolution, but for others (e.g., those with low slopes and small concavities), their Fourier behaviors may be similar. We hypothesize that the temporal evolution of the Fourier transform might be a useful tool to decipher the roles of nonlocal versus local, linear transport in other settings.

The reader will note that we have not offered a comparison between nonlinear diffusion and nonlocal transport. The nonlinearities in a nonlinear and nonlocal formulation result in similar behavior in wavenumber domain. There are some subtle differences in behavior; however, a discussion of these is beyond the scope of this paper. Insofar as the modeled land-surface profiles for nonlinear and nonlocal formulations are similar, so too are their spectral evolution. We address these similarities in the following section.

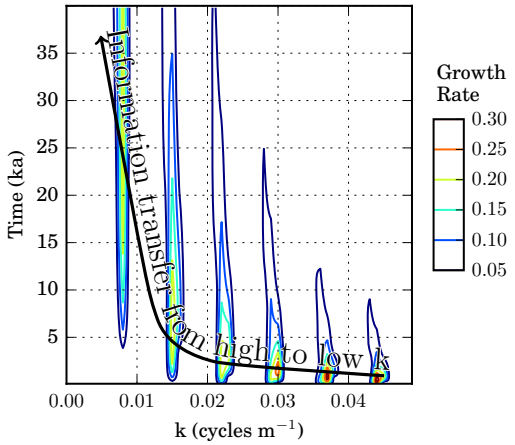

Figure 11. Plot of time versus spectral wavenumber k showing the temporal evolution of the growth rates of wavenumbers. Note that only positive growth rates are shown here for simplicity.

6 Discussion

6.1 Performance of nonlocal models

The results summarized in Table 1 show that the nonlocal flux formulation with only a positive, or downslope, component mimics the topographic evolution of the moraine better than other nonlocal models. Such models are consistent with the notion that a majority of transport is accomplished by dry ravel, which only mobilizes sediment in the downslope direction. That downslope-only flux models (nonlocal Case III) perform better may reflect that we use similar mathematics to describe upslope and downslope flux components in bi-directional flux models. It is likely, however, that the bulk downslope and upslope processes differ and may be better represented by different mathematics or parameters. For example, on these moraines most downslope motion may be due to dry ravel, whereas a smaller, but persistent upslope contribution may come from rainsplash. We expect that both entrainment rates and travel distance for rainsplash are functionally different from dry ravel. To test this scenario would require adding another set of parameters for the negative flux. To avoid being unnecessarily heuristic, we instead suggest that the downslope flux is much larger than the upslope component. This assumption may have an impact on the flux at locations with

low slopes, where the positive and negative flux contributions can be similar in magnitude. As such, this may partly explain the deviations we observe between observed and modeled profile forms for nonlocal transport at the crests and toes of moraines.

The spatial variation in grain size illustrated in Figure 5 could affect transport parameters in nonlocal and local formulations of transport. Recognizing that entrainment of particles requires a disturbance of sufficient energy to dislodge them, we suggest that smaller particles will be entrained by smaller disturbances which occur more frequently than the large ones required to move large particles. Therefore, a higher density of boulders might reduce entrainment E. However, we have somewhat arbitrarily determined boulders to be those greater than 25 cm in diameter whereas the impact on entrainment may be more accurately addressed by the distribution of grain sizes as opposed to the concentration of a single grain-size fraction. In addition, although the density of boulders is greater near the ridge, it may not be great enough to significantly alter the values for E. Further work might address the impact of grain size on either the entrainment rate or the pdf of travel distances [*DiBiase et al.*, 2017].

6.2 Comparison with local nonlinear flux description

The nonlinear transport model, (2), is a physically based model and is capable of capturing the essential behaviors of hillslope evolution and flux values. The success of (2) serves as motivation for the class of nonlocal models discussed here. That is, recognition of nonlinear dynamics brought attention to the idea that long-distance motions can contribute significantly to the hillslope sediment flux. Both classes of models are based on the notion that sediment particle travel distance is a key component of the flux yet they differ in their treatment of it. Given this similarity, nonlocal models ought to subsume nonlinear ones. There are, however, noteworthy differences between nonlocal and nonlinear models.

Recall that a nonlinear model is capable of nearly matching the result of a nonlocal model (Table 1), but to do so, $S_c = 0.8$. We have noted that locally, slopes exceed 0.8, meaning that the sediment flux at this location would be unrealistically large for a nonlinear model such as (2). However, a nonlinear model is not intended to be applied at scales smaller than the biogeomorphic scale of roughness present on hillslopes [*Roering et al.*, 2010]. Local formulations such as (2) and (13) require a spatial average of slope (window of 7-10 m according to *Roering et al.* [2010]), or alternatively, a time-averaged value at a location such that land-surface slope used in the models smoothly varies downslope. In contrast, nonlocal models remove this scale-dependence of slope [*Ganti et al.*, 2012] and do not explicitly require averaging. In this contribution we do use time-averaged values for slope; however, the mathematical development of the entrainment rate, $E(x')$ is based on the presence of biogeomorphic roughness creating locally over-steepened faces. In this sense, the formulation is acknowledging the presence of roughness in an implicit manner. Whereas a nonlocal model can in principle incorporate the biogeomorphic roughness present on hillslopes, we have not advanced the application at the relevant timescales or spatial resolution. However, now that we have demonstrated nonlocal transport at geomorphic timescales, future work might be well-suited to address shorter timescales and applying a nonlocal theory that explicitly includes the biogeomorphic roughness. Last, although we use a time-averaged slope here, the local slopes that we calculated do not exceed the limiting slope S_l, as they do in the nonlinear case.

In the case where $|S| > S_l$, a nonlocal formulation does not imply that the flux becomes infinite. The critical slope S_c in (2) represents a limiting situation where the flux nominally becomes very large, assuming sediment is available to be transported (in a time-averaged sense). In contrast, the critical slope S_c in the nonlocal formulation is to be interpreted as the slope at which sediment, once mobilized, does not become disentrained. In this situation where particle motions are not arrested, the flux is set by the upslope convolution of the entrainment volume, as in detachment-limited conditions [*Lamb et al.*, 2011].

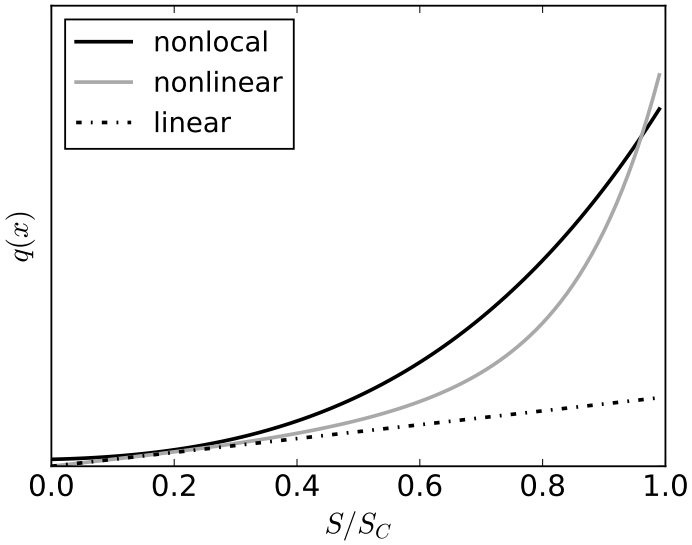

Figure 12. Plot of flux versus slope S/S_c based on the simplified versions of the nonlocal and nonlinear flux models together with the linear flux model. The flux values (y-axis) are only relative quantities depending on the choice of parameters. The nonlinear model here is approximated out to five terms.

6.3 Mapping Nonlocal to Nonlinear Flux Models

The different mathematics of nonlocal and nonlinear flux models prevent a straightforward comparison of the two. However, approximations of these models lead to identification of the essential behaviors which may be shared. To do so, we simplify both nonlinear and nonlocal flux models. For the simplification of nonlocal transport, we follow the steps of Furbish and Haff (2010) and approximate (3) with an advection-diffusion equation,

$$q(x)_{ad} = E(x)\mu_\lambda - \frac{\partial}{\partial x}\left[E(x)\sigma_\lambda\right], \tag{18}$$

where μ_λ and σ_λ^2 are the first and second moments of $f(r;x)$. Furthermore, Furbish and Haff (2010) show that the first term of (18) dominates, such that we can neglect the diffusive term. The expression for μ_λ is determined from a binomial expansion of $R(x-x',x')$. For a negative slope and with only downslope motions, the mean travel distance is

$$\mu_\lambda = \lambda_0\left(1-\frac{S}{S_l}\right)^2. \tag{19}$$

Using a nonlinear form for $E(x')$, the advective term of (18) is

$$q_a = E_0\lambda_0 - E_0\lambda_0\frac{2S}{S_l} + \left(\frac{E_0\lambda_0}{S_l^2} + E_1\lambda_0\right)S^2 - E_1\lambda_0\frac{2S^3}{S_l^2} + E_1\lambda_0\frac{S^4}{S_l^2}. \tag{20}$$

In comparison, the binomial expansion of the local nonlinear formulation leads to,

$$q_a = -D\left(S + \frac{S^3}{S_c^2} + \frac{S^5}{S_c^4} + \frac{S^7}{S_c^6} + \ldots\right). \tag{21}$$

Note that (21) contains only odd powers of S, whereas (20) contains consecutive integer powers of S. However, (20) and (21) do share a fundamental property in that they are both linear combinations of local nonlinear slope terms. Furthermore, we note that $E\lambda_0$ [$\mathrm{L}^2\ \mathrm{T}^{-1}$]

carries dimensions consistent with a hillslope diffusivity D, which suggests then that (20) can be mapped to a term of the same power in (21). Although there is a mismatch between approximated flux values (Figure 12), the basic form is the same. That these curves are approximations based on expansions, yet share the same form, provides an explanation for why nonlinear and nonlocal formulations lead to similar behaviors. Both the entrainment rate, E, and the disentrainment rate, P, are nonlinear functions of slope and both contribute to the nonlinear behavior of the sediment flux. However, we suggest that the key part of the nonlinearity appears to come from E. The shared behavior holds for $S \ll S_c$ and $S \ll S_l$. When $S \to S_c$ and $S \to S_l$ higher order terms in (21) become significant and (20) and (21) diverge.

6.4 Sensitivity to E and λ_0

The two central parameters for the nonlocal convolution integral flux formulation, E and λ_0, set the magnitude of sediment transport. These parameters hold real physical meaning that can be measured or modeled. This provides an opportunity to hypothesize about the impact of changing ecological or climatological conditions. For example, imagine a substantial shift in climate which drives an ecologic change from a grassland to a shrubland [*Pelletier et al.*, 2016]. Under these new conditions, long-distance transport events may become more common as there are fewer vegetative anchors for the soil which reflects an increase in E. Furthermore, this may increase the travel distance if patchy surface flows become a more prominent process, and which is represented by an increase in λ_0. Whereas the result of both changes is an increase in the flux, the response of the flux to each is not necessarily equal. Therefore, we question which parameters hold the most weight for a flux formulation as written in (3).

To investigate this we perform a sensitivity analysis. We make use of the Leibniz integral rule and take the derivative of the flux (9) with respect to E_1 and λ_0. To make this problem tractable, we must simplify the topography and imagine a hillslope with uniform slope, S, such that the spatial dependency of $E(x')$ and $R(x - x'; x')$ on x is removed. Furthermore, we conduct this analysis at a position beyond the saturation length of sediment transport. This represents a sensitivity analysis of the sediment flux some finite distance from the crest of a hillslope. We note that this is inherently a transient condition; however, it provides a simple and first-order estimate on the impact of key parametric values. We also point out that many slopes like the interior of a moraine are highly linear, thereby lending merit to this approach. Making these assumptions, the derivatives of (9) are

$$\frac{\mathrm{d}q(x)}{\mathrm{d}E_1} = \int_0^x S e^{-\frac{x-x'}{\lambda_0}\left(\frac{S_l+S}{S_l-S}\right)} \mathrm{d}x' \tag{22}$$

$$\frac{\mathrm{d}q(x)}{\mathrm{d}\lambda_0} = -\int_0^x \frac{E_1 S}{\lambda_0^2}\left(\frac{S_l+S}{S_l-S}\right)(x-x') e^{-\frac{x-x'}{\lambda_0}\left(\frac{S_l+S}{S_l-S}\right)} \mathrm{d}x'. \tag{23}$$

We can integrate (22) and (23) and neglect exponential terms that involve $\exp(-x/\lambda_0) \approx 0$, because we are sufficiently far downslope. This results in two, nearly identical nonlinear functional forms,

$$\frac{\mathrm{d}q(x)}{\mathrm{d}E_1} = \lambda_0 |S| \left(\frac{S_l - S}{S_l + S}\right) \quad S < 0 \tag{24}$$

$$\frac{\mathrm{d}q(x)}{\mathrm{d}\lambda_0} = E_1 |S| \left(\frac{S_l - S}{S_l + S}\right) \quad S < 0 \tag{25}$$

The flux is nonlinearly sensitive to both variables as slopes approach S_l. However, sensitivities differ based on the magnitude of the other variable in question. We should note the different units of (24) [L] and (25) [L T^{-1}], although a timescale is tied to (24), as λ_0 is the characteristic travel distance after a given time $\mathrm{d}t$. Insofar as lateral displacements, λ_0, are greater than the depth of entrained sediment per year, we see that the flux is more sensitive to E_1 than λ_0. For systems with higher E_1, the distribution of sediment becomes more significant in calculations of the flux. That is, if there is a lot of sediment in motion, emphasis should be placed on keeping track of it spatially; and if it travels far, then emphasis is placed on how much is in motion.

High sensitivity of the flux to E_1 is supported by the result presented in Figure 6, where surface of the cost function $C(E_1, \lambda_0)$ can be inferred from the paths taken by iterative choices of parameters. In particular, we emphasize that all paths converge to the same orientation before approaching the minimum of $C(E_1, \lambda_0)$. Furthermore, the orientation of that path is close to parallel with the λ_0 axis. These paths suggest that the cost surface contains a trough oriented along the λ_0 axis (denoted in Figure 6). This trough suggests that so long as the value of E_1 is correct, changes in λ_0 over up to an order of magnitude do little to change the form of the moraine. Although this indicates that the modeled hillslope form (not the flux) is more sensitive to changes in E_1, in order to correctly model the evolution of the land surface, one must first correctly describe the flux. Therefore, we interpret the geometry of $C(E_1, \lambda_0)$ as a reflection of the sensitivity of flux formulations to various transport parameters.

Consider a system with relatively small E_1 and a numerically larger λ_0. Now consider a significant but not large change in climate, namely, a shift that does not result in dramatic ecological changes. According to (24), depending on the value of λ_0 and on steep slopes, a slight shift in E_1 can lead to quite large increases in the flux. More specifically, the changes in the flux can be many times greater than the change in E_1. This type of analysis is similar to efforts that explore what values of the diffusivity-like rate constant D might take on in different settings. It is largely suggested that it varies as a function of climate and ecology [*Tucker and Bras*, 1998; *Istanbulluoglu and Bras*, 2005; *Hughes et al.*, 2009; *Pelletier et al.*, 2016]. However, this problem is a complex one that involves the specifics of ecology, geology, and climatology. The convolution integral forms of the nonlocal flux deconstruct rate constants like D into two physically interpretable parameters which are capable of addressing some of these specifics. This may provide an opportunity to theoretically address the impact of climate on hillslope sediment transport and erosion rates.

Through estimating a value of D for local linear diffusion, we show that, in this setting, the form of a moraine reflects only the time-averaged value of D (Appendix A). Previous work has demonstrated this concept [Figure 6, *Madoff and Putkonen*, 2016], although it has not addressed the mathematical basis. This is easily proven when the diffusion equation is examined in the wavenumber domain and is a point that may be significant in efforts to unfold the record of climate in hillslope form. To be clear, this concept only applies to topographic configurations that lack a boundary condition that reflects tectonic conditions (i.e. channel). There are numerous landforms for which there is no external forcing other than climate. For example, river terraces, faults scarps, and paleo-shorelines are all topographic features that lack externally forced boundary conditions, and therefore their evolution is driven only by climate. In such settings, under linear diffusion, their form would be expected to reflect a single value for D and contain no information about changing conditions. It remains unclear if a nonlinear formulation for sediment transport shares this property or not.

7 Conclusions

We have provided field-based evidence that demonstrates nonlocal sediment transport operating at the hillslope scale. By a measure of sum-of-squared differences, nonlocal hillslope sediment transport formulations reproduce observed profile forms with greater fidelity than local, linear diffusion. In particular we note that nonlocal formulations better describe the evolution of locations with large concavity. Nonlocal, convolution integral-based formulations match the performance of local nonlinear ones. We have shown that nonlinear and nonlocal formulations are expected to perform similarly as they are both motivated by the same theory, and mathematical simplifications highlight that the formulations share an underlying mathematical form.

In demonstrating the presence nonlocal sediment transport, we have obtained the first estimates of the parameters in the convolution integral-like flux formulation for sediment transport. Throughout this paper we have attempted to highlight that nonlocal formulations offer physically clear parameters that can potentially be measured in the field. Here we have

estimated the values for the time-averaged volumetric entrainment rate and a characteristic length-scale of particle travel distance. We find that time-averaged values for $E_1 \approx 0.01$ m/yr and $\lambda_0 \approx 0.35$ m. This implies that, on average, the thickness of the slice of sediment that is entrained annually in this setting goes from zero to one cm as slopes go from zero to one. The interpretation of λ_0 is that this nominally represents the average total (uni-directional) displacement of particles entrained (perhaps multiple times) on a flat surface during one year.

We have questioned which parameter is most influential for the volumetric sediment flux. A sensitivity analysis reveals that the flux depends most heavily on the slope-dependent term of the entrainment rate. That the entrainment dominates the flux is consistent with research on bedload sediment transport where changes in particle activity primarily control changes in the sediment flux, not hop distance lengths [*Ancey et al.*, 2008; *Radice et al.*, 2009; *Ancey*, 2010; *Roseberry et al.*, 2012]. Insofar as the entrainment rate, E, dominates the flux at our field site, we expect that future efforts aimed at empirically or theoretically determining values for E would be worthwhile.

We have identified behaviors in wavenumber domain that distinguish between local linear diffusion and nonlocal/nonlinear formulations. Whereas all transport models result in an overall decay of topographic variance, the way in which this decay occurs differs. Linear diffusion shows that spectral amplitude contained in every wave-number must decrease. Nonlinear and nonlocal models destroy topographic variance by concentrating spectral amplitude to low wavenumbers. In doing so, spectral amplitude in certain wavenumbers can temporarily grow, thereby providing a unique signature. These signatures have some potential as being tools to identify the style of sediment transport that has occurred during a landform or landscape's history.

Notation

- x position (L)
- x' up or downslope position (L)
- ζ land-surface elevation (L)
- t time (T)
- q volumetric sediment flux ($L^2\ T^{-1}$)
- D hillslope diffusivity (linear and nonlinear) ($L^2\ T^{-1}$)
- S land-surface slope
- S_c critical slope (nonlinear)
- E volumetric entrainment rate ($L^3\ L^{-2}\ T^{-1}$)
- E_0 background entrainment rate ($L^3\ L^{-2}\ T^{-1}$)
- E_1 slope-modulating entrainment rate ($L^3\ L^{-2}\ T^{-1}$)
- α slope-dependency of the entrainment rate
- R survival function
- P disentrainment rate [L^{-1}]
- r travel distance (L)
- f probability density function of travel distance (L^{-1})
- λ_0 characteristic particle travel distance (L)
- S_l limiting slope on which particles do not stop (nonlocal)
- q_p volumetric sediment flux in positive x direction ($L^2\ T^{-1}$)
- q_n volumetric sediment flux in negative x direction ($L^2\ T^{-1}$)
- p probability of moving in positive x direction
- n probability of moving in negative x direction
- S_p threshold slope above which all particles move in one direction
- Z Fourier transform of the land-surface elevation (L^2)
- k wavenumber (L^{-1})
- C_f cost function, sum-of-squared deviations (L^2)

κ approximating kernel
ϕ_l decay constant for approximating kernel (L^{-1})
w_l weighting function associated with approximating kernel $\kappa(\phi_l)$
q_{ad} approximated nonlocal flux in advection-diffusion form ($L^2\ T^{-1}$)
μ_λ mean travel distance [L]
σ_λ variance of travel distance [L^2]

A: Why moraine form reflects time-averaged value of *D*

The Fourier transform of a one-dimensional signal (e.g., land surface) undergoing linear diffusion has the solution

$$Z(k,T_1) = Z(k,0)e^{-k^2 D_0 T_0}, \tag{A.1}$$

where $Z(k,0)$ is the initial transform and D_0 is the diffusivity over the time interval T_0 ending at the start of the next interval T_1. The Fourier transform after successive time intervals with different values of D are

$$Z(k,T_2) = Z(k,T_1)e^{-k^2 D_1 T_1} \tag{A.2}$$

$$Z(k,T_3) = Z(k,T_2)e^{-k^2 D_2 T_2} \qquad \text{etc.} \tag{A.3}$$

Using these definitions, we can recursively substitute expressions for $Z(k,T_n)$ to give, for example,

$$\begin{aligned} Z(k,T_3) &= Z(k,0)e^{-k^2 D_0 T_0} e^{-k^2 D_1 T_1} e^{-k^2 D_2 T_2} \\ &= Z(k,0)e^{-k^2 (D_0 T_0 + D_1 T_1 + D_2 T_2)}. \end{aligned} \tag{A.4}$$

In general we may choose $\Delta T = T_0 = T_1 = T_2 = \ldots$ so that the total time $T = n\Delta T$ and $D_0T_0 + D_1T_1 + D_2T_2 + \ldots = (D_0 + D_2 + D_3 + \ldots)\Delta T = (D_0 + D_2 + D_3 + \ldots)T/n = \overline{D}T$, where $\overline{D} = (D_0 + D_2 + D_3 + \ldots)/n$ is the time-averaged diffusivity. Then,

$$Z(k,T) = Z(k,0)e^{-k^2 \overline{D} T}. \tag{A.5}$$

Note that because (A.4) is additive, the order in which the values of D appear is unimportant. In the limit of $\Delta T \rightarrow 0$, the formulation represents the outcome of a smooth (rather than discrete) variation in D (e.g., Box and Jenkins, 1976 p.355-362).

Acknowledgments
We acknowledge support by the National Science Foundation (EAR-1420831 to DJF and DJM, EAR-1420898 to JJR). We thank Amanda Keen-Zebert for thoughtful discussion and aid in the field. Timothy Watkins and Sarah Sams were also instrumental in helping with field work. We thank Vamsi Ganti and two anonymous reviewers for thoughtful comments that helped clarify this work.

References

Ancey, C., A. Davison, T. Böhm, M. Jodeau, and P. Frey (2008), Entrainment and motion of coarse particles in a shallow water stream down a steep slope, *J. of Flu. Mech.*, *595*, 83–114, doi:10.1017/S0022112007008774.

Ancey, C. (2010), Stochastic modeling in sediment dynamics: Exner equation for planar bed incipient bed load transport conditions, *J. of Geophys. Res.: E Surf.*, 115, F00A11, doi: 10.1029/2009JF001260.

Anderson, R. S. (2002), Modeling the tor-dotted crests, bedrock edges, and parabolic profiles of high alpine surfaces of the Wind River Range, Wyoming, *Geomorphology*, *46*(1), 35–58

Anderson, R. S. (2015), Particle trajectories on hillslopes: Implications for particle age and 10be structure, *J.of Geophys. Res.: Earth Surf.*, *120*(9), 1626–1644, doi: 10.1002/2015JF003479.

Box, G. E., G. M. Jenkins, G. C. Reinsel, and G. M. Ljung (1976), *Time series analysis: forecasting and control*, John Wiley & Sons.

Carretier, S., P. Martinod, M. Reich, and Y. Godderis (2016), Modelling sediment clasts transport during landscape evolution, *Earth Surf. Dyn.*, *4*(1), 237–251, doi:10.5194/esurf-4-237-2016.

Carslaw, H. S., and J. C. Jaeger (1959), Conduction of heat in solids, *Oxford University Press, 2nd ed.*, New York, NY.

Carson, M. A., and M. J. Kirkby (1972), *Hillslope form and process*, vol. 475, Cambridge University Press, New York, NY.

Culling, W. (1963), Soil creep and the development of hillside slopes, *J. of Geol.*, *71*(2), 127–161

DiBiase, R. A., K. X. Whipple, A. M. Heimsath, and W. B. Ouimet (2010), Landscape form and millennial erosion rates in the San Gabriel Mountains, CA, *Earth and Planet. Sci. Lett.*, *289*(1), 134–144 ,doi:10.1016/j.epsl.2009.10.036.

DiBiase, R. A., and M. P. Lamb (2013), Vegetation and wildfire controls on sediment yield in bedrock landscapes *Geophys. Res. Lett.*, *40*(6), 1093–1097,doi:10.1002/grl.50277.

DiBiase, R. A., M. P. Lamb, V. Ganti, and A. M. Booth (2017), Slope, grain size, and roughness controls on dry sediment transport and storage on steep hillslopes, *J. of Geophys. Res.: Earth Surf.*, 2016JF003970, doi:10.1002/2016JF003970, .

Domaradzki, J. A., and R. S. Rogallo (1990), Local energy transfer and nonlocal interactions in homogeneous, isotropic turbulence, *Phys. of Fluids A: Fluid Dynam.*, *2*(3), 413–426.

Dunne, T., D. V. Malmon, and S. M. Mudd (2010), A rain splash transport equation assimilating field and laboratory measurements, *J. of Geophys. Res.: Earth Surf.*, *115*, F01001, doi:10.1029/2009JF001302.

Fathel, S. L., D. J. Furbish, and M. W. Schmeeckle (2015), Experimental evidence of statistical ensemble behavior in bed load sediment transport, *J. of Geophys. Res.: Earth Surf.*, *120*(11), 2298–2317, doi:10.1002/2015JF003552.

Fernandes, N. F., and W. E. Dietrich (1997), Hillslope evolution by diffusive processes: The timescale for equilibrium adjustments, *Water Res. Res.*, *33*(6), 1307–1318.

Foufoula-Georgiou, E., V. Ganti, and W. Dietrich (2010), A nonlocal theory of sediment transport on hillslopes, *J. of Geophys. Res.: Earth Surf.*, *115*, F00A16, doi: 10.1029/2009JF001280.

Furbish, D. J. (2003), Using the dynamically coupled behavior of land-surface geometry and soil thickness in developing and testing hillslope evolution models, in *Prediction in Geomorphology, Geophys. Monogr. Ser.*, vol. 135, edited by P.R. Wilcock and I.M. Iverson, pp. 169–181, AGU, Washington, D.C.

Furbish, D. J., and P. K. Haff (2010), From divots to swales: Hillslope sediment transport across divers length scales, *J. of Geophys. Res.: Earth Surf.*, *115*, F03001, doi: 10.1029/2009JF001576.

Furbish, D. J., and J. J. Roering (2013), Sediment disentrainment and the concept of local versus nonlocal transport on hillslopes, *J. of Geophys. Res.: Earth Surf.*, 118, 937–952, doi:10.1002/jgrf.20071.

Furbish, D. J., P. K. Haff, W. E. Dietrich, and A. M. Heimsath (2009a), Statistical description of slope-dependent soil transport and the diffusion-like coefficient, *J. of Geophys. Res.: Earth Surf.*, *114*, F00A05, doi:10.1029/2009JF001267.

Furbish, D. J., E. M. Childs, P. K. Haff, and M. W. Schmeeckle (2009b), Rain splash of soil grains as a stochastic advection-dispersion process, with implications for desert plant-soil interactions and land-surface evolution, *J. of Geophys. Res.: Earth Surf.*, *114*, F00A03, doi:10.1029/2009JF001265.

Furbish, D. J., P. K. Haff, J. C. Roseberry, and M. W. Schmeeckle (2012), A probabilistic description of the bed load sediment flux: 1. theory, *J. of Geophys. Res.: Earth Surf.*, *117*,

F03031, doi:10.1029/2012JF002352.

Gabet, E. J. (2003), Sediment transport by dry ravel, *J. of Geophys. Res.: Sol. Earth*, *108*(B1), 2049, doi:10.1029/2001JB001686.

Gabet, E. J., and M. K. Mendoza (2012), Particle transport over rough hillslope surfaces by dry ravel: Experiments and simulations with implications for nonlocal sediment flux, *J. of Geophys. Res.: Earth Surf.*, *117*, F01019, doi:10.1029/2011JF002229.

Gabet, E. J., O. Reichman, and E. W. Seabloom (2003), The effects of bioturbation on soil processes and sediment transport, *Ann. Rev. of Earth and Planet. Sci.*, *31*(1), 249–273, doi:10.1146/annurev.earth.31.100901.141314.

Gabet, E. J., et al. (2000), Gopher bioturbation: Field evidence for non-linear hillslope diffusion, *Earth Surf. Proc. and Land.*, *25*(13), 1419–1428.

Ganti, V., P. Passalacqua, and E. Foufoula-Georgiou (2012), A sub-grid scale closure for nonlinear hillslope sediment transport models, *J. of Geophys. Res.: Earth Surf.*, *117*(F2), F02012, doi:10.1029/2011JF002181.

Gilad, E., and J. Von Hardenberg (2006), A fast algorithm for convolution integrals with space and time variant kernels, *J. of Comput. Phys.*, *216*(1), 326–336, doi:10.1016/j.jcp.2005.12.003.

Hellmer, M. C., B. A. Rios, W. B. Ouimet, and T. R. Sibley (2015), Ice storms, tree throw, and hillslope sediment transport in northern hardwood forests, *Earth Surf. Proc. and Land.*, *40*, 901–912, doi:10.1002/esp.3690.

Heyman, J., P. Bohorquez, and C. Ancey (2016), Entrainment, motion and deposition of coarse particles transported by water over a sloping mobile bed, *J. of Geophys. Res.: Earth Surf.*, *121*, 1931–1952, doi:10.1002/2015JF003672.

Hornberger, G., and P. Wiberg (2004), Finite Difference Solutions for Transient Problems, in *Numerical methods in hydrological sciences*, 8.1 – 8.20, American Geophysical Union, Washington, D.C., doi:10.1029/001LN03.

Hughes, M. W., P. C. Almond, and J. J. Roering (2009), Increased sediment transport via bioturbation at the last glacial-interglacial transition, *Geol.*, *37*(10), 919–922, doi:10.1130/G30159A.1.

Istanbulluoglu, E., and R. L. Bras (2005), Vegetation-modulated landscape evolution: Effects of vegetation on landscape processes, drainage density, and topography, *J. of Geophys. Res.: Earth Surf.*, *110*(F2), F02012, doi:10.1029/2004JF000249.

Johnson, M. O., S. M. Mudd, B. Pillans, N. A. Spooner, L. Keith Fifield, M. J. Kirkby, and M. Gloor (2014), Quantifying the rate and depth dependence of bioturbation based on optically-stimulated luminescence (osl) dates and meteoric 10be, *Earth Surf. Proc. and Land.*, *39*(9), 1188–1196, doi:10.1002/esp.3520.

Jyotsna, R., and P. Haff (1997), Microtopography as an indicator of modern hillslope diffusivity in arid terrain, *Geol.*, *25*(8), 695–698.

Kaufman, D. S., S. C. Porter, and A. R. Gillespie (2003), Quaternary alpine glaciation in Alaska, the Pacific northwest, Sierra Nevada, and Hawaii, *Dev. Quat. Sci*, *1*, 77–103, doi:10.1016/S1571-0866(03)01005-4.

Kirkby, M., and I. Statham (1975), Surface stone movement and scree formation, *J. of Geol.*, *83*(3), 349–362.

Lamb, M. P., J. S. Scheingross, W. H. Amidon, E. Swanson, and A. Limaye (2011), A model for fire-induced sediment yield by dry ravel in steep landscapes, *J. of Geophys. Res.: Earth Surf.*, *116*(F3), F03006, doi:10.1029/2010JF001878.

Lamb, M. P., M. Levina, R. A. DiBiase, and B. M. Fuller (2013), Sediment storage by vegetation in steep bedrock landscapes: Theory, experiments, and implications for postfire sediment yield, *J. of Geophys. Res.: Earth Surf.*, *118*(2), 1147–1160, doi:10.1002/jgrf.20058.

Madoff, R. D., and J. Putkonen (2016), Climate and hillslope degradation vary in concert; 85ka to present, eastern Sierra Nevada, CA, USA, *Geomorphology*, *266*, 33–40 doi:10.1016/j.geomorph.2016.05.010.

Martin, R. L., D. J. Jerolmack, and R. Schumer (2012), The physical basis for anomalous diffusion in bed load transport, *J.of Geophys. Res.: Earth Surf.*, *117*(F1), F01018, doi:

10.1029/2011JF002075.

McGuire, L. A., J. D. Pelletier, and J. J. Roering (2014), Development of topographic asymmetry: Insights from dated cinder cones in the western United States, *J. of Geophys.l Res.: Earth Surf.*, *119*(8), 1725–1750, doi:10.1002/2014JF003081.

Mensing, S. A. (2001), Late-glacial and early holocene vegetation and climate change near Owens Lake, eastern California, *Quat. Res.*, *55*(1), 57–65, doi:10.1006/qres.2000.2196.

Michaelides, K., I. Ibraim, G. Nord, and M. Esteves (2010), Tracing sediment redistribution across a break in slope using rare earth elements, *Earth Surf. Proc. and Land.*, *35*(5), 575–587, doi:10.1002/esp.1956.

Michaelides, K., and G.J. Martin (2012), Sediment transport by runoff on debris-mantled dryland hillslopes, *J. of Geophys. Res.: Earth Surf.*, *117*, F03014, doi: 10.1029/2012JF002415.

Morgan, D., and J. Putkonen (2012), Moraine degradation rates quantified with cosmogenic be-10 from soil profiles in Bloody Canyon, paper presented at Geological Society of America Annual Meeting, Charlotte, NC.

Mudd, S. M., and D. J. Furbish (2007), Responses of soil-mantled hillslopes to transient channel incision rates, *J. of Geophys. Res.: Earth Surf.*, *112*(F3), F03S18, doi: 10.1029/2006JF000516.

Ouimet, W. B., K. X. Whipple, and D. E. Granger (2009), Beyond threshold hillslopes: Channel adjustment to base-level fall in tectonically active mountain ranges, *Geology*, *37*(7), 579–582, doi:10.1130/G30013A.1.

Parker, G., C. Paola, and S. Leclair (2000), Probabilistic exner sediment continuity equation for mixtures with no active layer, *J. of Hydraul. Eng.*, *126*(11), 818–826.

Pelletier, J. D., M. H. Nichols, and M. A. Nearing (2016), The influence of holocene vegetation changes on topography and erosion rates: a case study at walnut gulch experimental watershed, arizona, *Earth Surf. Dyn.*, *4*(2), 471–488, doi:10.5194/esurf-4-471-2016.

Phillips, F. M., M. G. Zreda, S. S. Smith, D. Elmore, P. W. Kubik, and P. Sharma (1990), Cosmogenic chlorine-36 chronology for glacial deposits at bloody canyon, eastern sierra nevada, *Science*, *248*(4962), 1529–1532.

Phillips, F. M., M. Zreda, M. A. Plummer, D. Elmore, and D. H. Clark (2009), Glacial geology and chronology of bishop creek and vicinity, eastern sierra nevada, california, *Geol. Soc. of Amer. Bull.*, *121*(7-8), 1013–1033, , doi:10.1130/B26271.1.

Poularikas, A. D. (1998), *Handbook of formulas and tables for signal processing*, vol. 13, Springer-Verlag Berlin Heidelberg.

Putkonen, J., J. Connolly, and T. Orloff (2008), Landscape evolution degrades the geologic signature of past glaciations, *Geomorphology*, *97*(1), 208–217, doi: 10.1016/j.geomorph.2007.02.043.

Putkonen, J., D.J Morgan, and G. Balco (2012), Regolith transport quantified by braking block, McMurdo Dry Valleys, Antarctica, *Geomorphology*, *155*, 80–87, doi: 10.1016/j.geomorph.2011.12.010.

Radice, A., F. Ballio, and V. Nikora (2009), On statistical properties of bed load sediment concentration, *Water Res. Res*, *45*(6), W06501, doi:10.1029/2008WR007192.

Roering, J. J., J. W. Kirchner, and W. E. Dietrich (1999), Evidence for nonlinear, diffusive sediment transport on hillslopes and implications for landscape morphology, *Water Res. Res.*, *35*(3), 853–870.

Roering, J. J., P. Almond, P. Tonkin, and J. McKean (2004), Constraining climatic controls on hillslope dynamics using a coupled model for the transport of soil and tracers: Application to loess-mantled hillslopes, South Island, New Zealand, *J. of Geophys. Res.: Earth Surf.*, *109*(F1), F01010, doi:10.1029/2003JF000034.

Roering, J. J., J. T. Perron, and J. W. Kirchner (2007), Functional relationships between denudation and hillslope form and relief, *Earth and Planet. Sci. Lett.*, *264*(1), 245–258, doi: 10.1016/j.epsl.2007.09.035.

Roering, J. J., J. Marshall, A. M. Booth, M. Mort, and Q. Jin (2010), Evidence for biotic controls on topography and soil production, *Earth and Planet. Sci. Lett.*, *298*(1), 183–190,

doi:10.1016/j.epsl.2010.07.040.

Rood, D. H., D. W. Burbank, and R. C. Finkel (2011), Chronology of glaciations in the Sierra Nevada, California, from 10 be surface exposure dating, *Quat. Sci. Rev.*, *30*(5), 646–661, doi:10.1016/j.quascirev.2010.12.001.

Roseberry, J. C., M. W. Schmeeckle, and D. J. Furbish (2012), A probabilistic description of the bed load sediment flux: 2. particle activity and motions, *J. of Geophys. Res.: Earth Surf.*, *117*(F3), F03032, doi:10.1029/2012JF002353.

Schaefer, J. M., G. H. Denton, D. J. Barrell, S. Ivy-Ochs, P. W. Kubik, B. G. Andersen, F. M. Phillips, T. V. Lowell, and C. Schlüchter (2006), Near-synchronous interhemispheric termination of the last glacial maximum in mid-latitudes, *Science*, *312*(5779), 1510–1513, doi:10.1126/science.1122872.

Schumer, R., M. M. Meerschaert, and B. Baeumer (2009), Fractional advection-dispersion equations for modeling transport at the earth surface, *J. of Geophys. Res.: Earth Surf.*, *114*(F4), F00A07, doi:10.1029/2008JF001246.

Shelef, E., and G. E. Hilley (2016), A unified framework for modeling landscape evolution by discrete flows, *J. of Geophys. Res.: Earth Surf.*, *121*, 816–842, doi:10.1002/2015JF003693.

Tucker, G. E., and D. N. Bradley (2010), Trouble with diffusion: Reassessing hillslope erosion laws with a particle-based model, *J. of Geophys. Res.*, *115*, F00A10, doi:10.1029/2009JF001264.

Tucker, G. E., and R. L. Bras (1998), Hillslope processes, drainage density, and landscape morphology, *Water Res. Res.*, *34*(10), 2751–2764.